Catalytic Activity of MCM-48-, SBA-15-, MCF-, and MSU-Type Mesoporous Silicas Modified with Fe^{3+} Species in the Oxidative Dehydrogenation of Ethylbenzene in the Presence of N_2O

Piotr Kuśtrowski,*,† Lucjan Chmielarz,† Janusz Surman,† Ewa Bidzińska,† Roman Dziembaj,† Pegie Cool,‡ and Etienne F. Vansant‡

Jagiellonian University, Faculty of Chemistry, Ingardena 3, 30-060 Kraków, Poland, and University of Antwerp, Department of Chemistry, Laboratory of Adsorption and Catalysis, Universiteitplein 1, 2610 Wilrijk, Belgium

Received: June 29, 2005; In Final Form: August 20, 2005

MCM-48, SBA-15, MCF, and MSU mesoporous silicas were used as supports for a deposition of Fe oxide species. Iron was introduced using two different methods: the wetness impregnation and the molecular designed dispersion (MDD). The obtained catalysts were characterized with respect to their textural parameters (BET), chemical composition (electron microprobe analysis), and reducibility (TPR). The coordination environment of Fe was determined using EPR and UV−vis/DRS. The samples were tested as catalysts in the oxidative dehydrogenation of ethylbenzene to styrene in the presence of N_2O. An influence of Fe dispersion and reducibility on the catalytic activity was discussed. Isolated Fe^{3+} species appeared to be more selective in the styrene formation, whereas iron oxide clusters showed a higher selectivity in total oxidation of aromatic hydrocarbons. The reaction system was well described by the Mars− van Krevellen mechanism.

Introduction

Styrene, an important monomer in polymerization processes, is mainly produced by thermodynamically limited dehydrogenation of ethylbenzene (EB) over a potassium-doped hematite catalyst.[1] Because of an endothermic effect, this reaction is carried out at elevated temperatures (550−650 °C) in the presence of excess superheated water vapor, which is used to supply the heat of reaction and shift the equilibrium to higher styrene yields by a decrease in the partial pressures of reactants.[2] The thermodynamic limitation and high endothermic effect of the EB dehydrogenation are the reasons for searching alternative routes in styrene production. The oxidative dehydrogenation of ethylbenzene, based on an introduction of an oxidant to the EB feed, seems to be one of the promising methods.[2−5] The oxidative dehydrogenation process is exothermic so that it can be carried out at a lower temperature as compared to the classical EB dehydrogenation and, additionally, is not equilibrium-limited. Oxygen was first proposed to be used as an oxidizing agent. However, it appeared that a large amount of aromatic compounds was totally oxidized to CO_x, when oxygen was applied. Other oxidants (e.g., SO_2, nitrobenzene, CO_2, and N_2O) were therefore tested in the oxidative dehydrogenation of EB. Coupling the N_2O decomposition with the EB dehydrogenation, which has been proposed recently,[6,7] seems to be a very effective and selective process for styrene production. The preliminary studies showed that the most promising catalysts are based on Cu-, Fe-, and Cr-oxide on γ-Al_2O_3 and mesoporous silicas (SBA-15, MCF, MCM-48, and MSU) varying in textural properties. However, the Fe-modified catalysts were characterized by a high activity and selectivity. Furthermore, it was observed that the isolated Fe^{3+} species catalyzed the EB dehydrogenation more effectively than the Fe clusters.[7]

All Fe-containing catalysts studied in our previous papers[6,7] were prepared by the impregnation technique. It could be expected, however, that using the grafting method for the modification of silica support should improve the Fe dispersion. In the present work, two different modification methods of the mesoporous silicas (SBA-15, MCF, MCM-48, and MSU) with iron are compared in relation to their catalytic activity in the oxidative dehydrogenation of EB. The Fe-containing catalysts were prepared by the impregnation technique and the molecular designed dispersion (MDD) method. The MDD method is one of the grafting techniques that is very helpful in a tuned deposition of active components on the support surface.[8−12] This method consists of two steps. First, a transition metal acetylacetonate complex is grafted on a support surface. Two different mechanisms of the interaction between the complex and the surface can be considered: (1) by hydrogen bonding between the acetylacetonate ligand and a surface silanol group and (2) by a ligand exchange with a formation of a covalent $Me-O_{support}$ bond. In the subsequent step, the adsorbed complex is thermally decomposed to obtain a transition metal oxide species at the surface.

Experimental Procedures

Catalyst Preparation. Mesoporous silicas (SBA-15, MCF, MCM-48, and MSU) were used as supports for the iron oxide active phase. For the synthesis of MCM-48, 2.89 g of a $C_{16-12-16}$ Gemini and 0.35 g of NaOH were dissolved in 60.0 mL of distilled water and stirred until the surfactant was dissolved.[13] Then, 2 g of fumed silica (Aerosil 380) was added under vigorous stirring. After 30 min of mixing at room temperature, the resulting gel was transferred into an autoclave and aged at 130 °C for 3 days. Subsequently, it was filtered, washed with

* To whom correspondence should be addressed. Tel.: +48 12 6632006; fax: +48 12 6340515; e-mail: kustrows@chemia.uj.edu.pl.
† Jagiellonian University.
‡ University of Antwerp.

10.1021/jp0535442 CCC: $30.25
Published on Web 10/12/2005

TABLE 1: Textural Parameters and Fe Loading of the Studied Mesoporous Materials

sample	S_{BET} [m^2/g]	V_{total} [cm^3/g]	av pore diameter [Å]	total Fe loading [wt %]	content of isolated Fe^{3+} species [%]
MCM-48	909	1.08	38		
Feimp/MCM-48	734	0.85	36	0.7	52
Fe4/MCM-48	850	1.00	36	1.6	72
Fe12/MCM-48	866	1.01	36	2.7	75
SBA-15	773	0.85	78		
Feimp/SBA-15	707	0.76	78	0.6	67
Fe4/SBA-15	764	0.85	78	1.7	92
Fe12/SBA-15	730	0.82	78	2.2	86
MCF	698	2.35	260		
Feimp/MCF	576	2.21	260	0.7	66
Fe4/MCF	629	2.20	260	1.7	88
Fe12/MCF	585	2.22	260	2.2	92
MSU	271	0.78	114		
Feimp/MSU	247	0.75	112	0.6	24
Fe4/MSU	259	0.72	114	2.1	100
Fe12/MSU	250	0.68	114	2.4	100

30 mL of distilled water, and resuspended in distilled water (30 mL) for 24 h at 130 °C. This procedure was carried out twice. The final product was separated by filtration, washed with distilled water, and dried at room temperature.

Mesoporous silica SBA-15 was synthesized according to the procedure described earlier by Van Bavel et al.[14] A total of 4.0 g of poly(ethylene oxide)-*block*-poly(propylene oxide)-*block*-poly(ethylene oxide) triblock copolymer ($EO_{20}PO_{70}EO_{20}$, Pluronic P123) was dissolved in 1.6 M HCl (150 mL), and then 9.14 mL of tetraethyl orthosilicate (TEOS) was added. The obtained suspension was stirred at 45 °C for 8 h and then aged at 80 °C for 15 h. The solid product was filtered, washed with distilled water, and dried at room temperature.

The synthesis method of MCF was given previously by Schmidt-Winkel et al.[15] A total of 4.0 g of Pluronic P123 was dissolved in 150 mL of aqueous HCl solution (1.6 M) at 35−40 °C. Then, NH_4F (46.7 mg) and 1,3,5-trimethylbenzene (mesitylene, 2.0 g) were added and vigorously stirred for 1 h. Subsequently, tetraethyl orthosilicate (TEOS, 9.14 mL) was added. After 20 h at 35−40 °C, the slurry was transferred to an autoclave and aged at 100 °C for 24 h. The obtained precipitate was filtered, washed with distilled water, and dried in air.

The synthesis of MSU was performed using a modified procedure described by Kim et al.[16] Sodium silicate (11.8 mL) was dissolved in 278 mL of distilled water and mixed with 0.22 M brij 56 (5.5 mL) and acetic acid (2.5 mL). After 1 h, NaF (0.06 g) was added, and the resulting gel was left at 60 °C for 3 days under vigorous stirring. Finally, the white product was filtered, washed with distilled water, and dried at room temperature.

Prior to the modification with transition metal complexes, the samples were calcined at 550 °C with a heating rate of 1 °C/min and an isothermal period of 8 h in air.

The first series of supported catalysts was prepared by an impregnation technique using solutions of $Fe(NO_3)_3 \cdot 9H_2O$ (Fluka). The amount of iron nitrate was adjusted to obtain a transition metal content in the catalysts equal to 1.0 wt %. The obtained precursors were dried at room temperature for 3 days and then calcined in air at 450 °C for 3 h. The samples prepared by the impregnation technique are denoted as Feimp/support.

The liquid-phase MDD method was used for the modification of mesoporous silicas with iron oxide as well. Deposition of iron acetylacetonate was performed in a dry nitrogen glovebox.

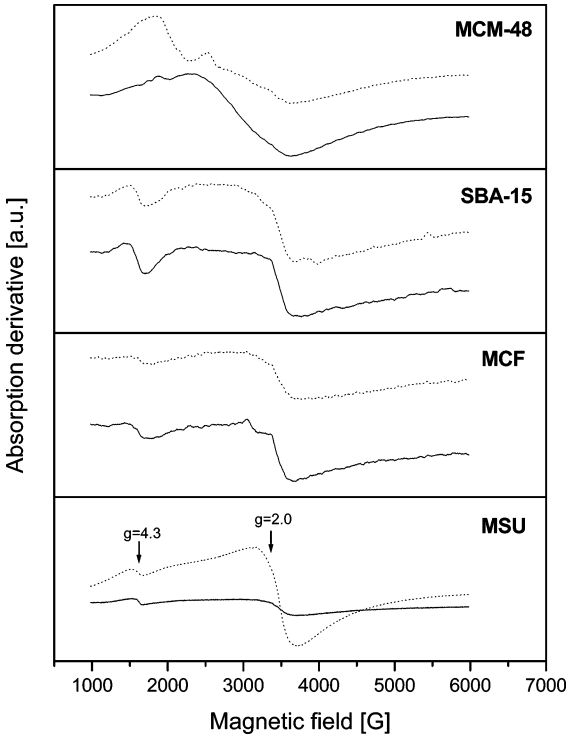

Figure 1. EPR spectra of the mesoporous silicas modified with Fe by impregnation (solid line) or by grafting at higher $Fe(acac)_3$ concentrations (dotted line).

One gram of the thermally treated support was stirred at room temperature in zeolite-dried toluene (100 mL) containing 0.04 mmol (the samples denoted as Fe4/support) or 0.12 mmol (the samples denoted as Fe12/support) of $Fe(acac)_3$. The total time of the deposition was 1 h. The modified supports were filtered and washed 5 times with fresh solvent to remove the excess of the metal acac complex. A washing cycle consisted of washing 1 g of the deposited sample with an aliquot of 25 mL of toluene.[12] The sample was dried under vacuum at room temperature. Finally, the material was calcined at 550 °C with a heating rate of 1 °C/min and an isothermal period of 8 h in air atmosphere.

Characterization Techniques. Fe loadings were determined by electron microprobe analysis performed on a JEOL Superprobe 733. Textural parameters of the calcined samples were determined by N_2 sorption at −196 °C using an ASAP 2010 (Micromeritics) after outgassing the materials under vacuum at 200 °C for 16 h. EPR measurements were performed with a Bruker ELEXSYS 500 spectrometer (Karlsruhe, Germany) operating in X-band (9.2 GHz) at a modulation frequency of 100 kHz. The EPR spectra were recorded at room temperature with a modulation of 5 mT and a microwave power of 10 mW. The EPR measurements were performed with the calcined samples after outgassing at 120 °C for 2 h. UV−vis diffuse reflectance (UV−vis/DRS) analysis was carried out on a Nicolet Evolution 500 spectrophotometer. The spectra were taken in the range of 200−800 nm for the calcined samples (2 wt %) diluted in KBr.

Temperature-programmed reduction (TPR) of the catalysts was carried out in the temperature range of 100−1000 °C in a fixed bed continuous flow quartz microreactor. The flow of the reduction mixture was controlled by a mass flow controller (Brooks 5850^E). The hydrogen consumption was monitored online by a thermal conductivity detector (TCD) connected to the reactor outlet by a heated line. Prior to the TPR experiments, a sample of 50 mg of calcined catalyst was outgassed at 200 °C

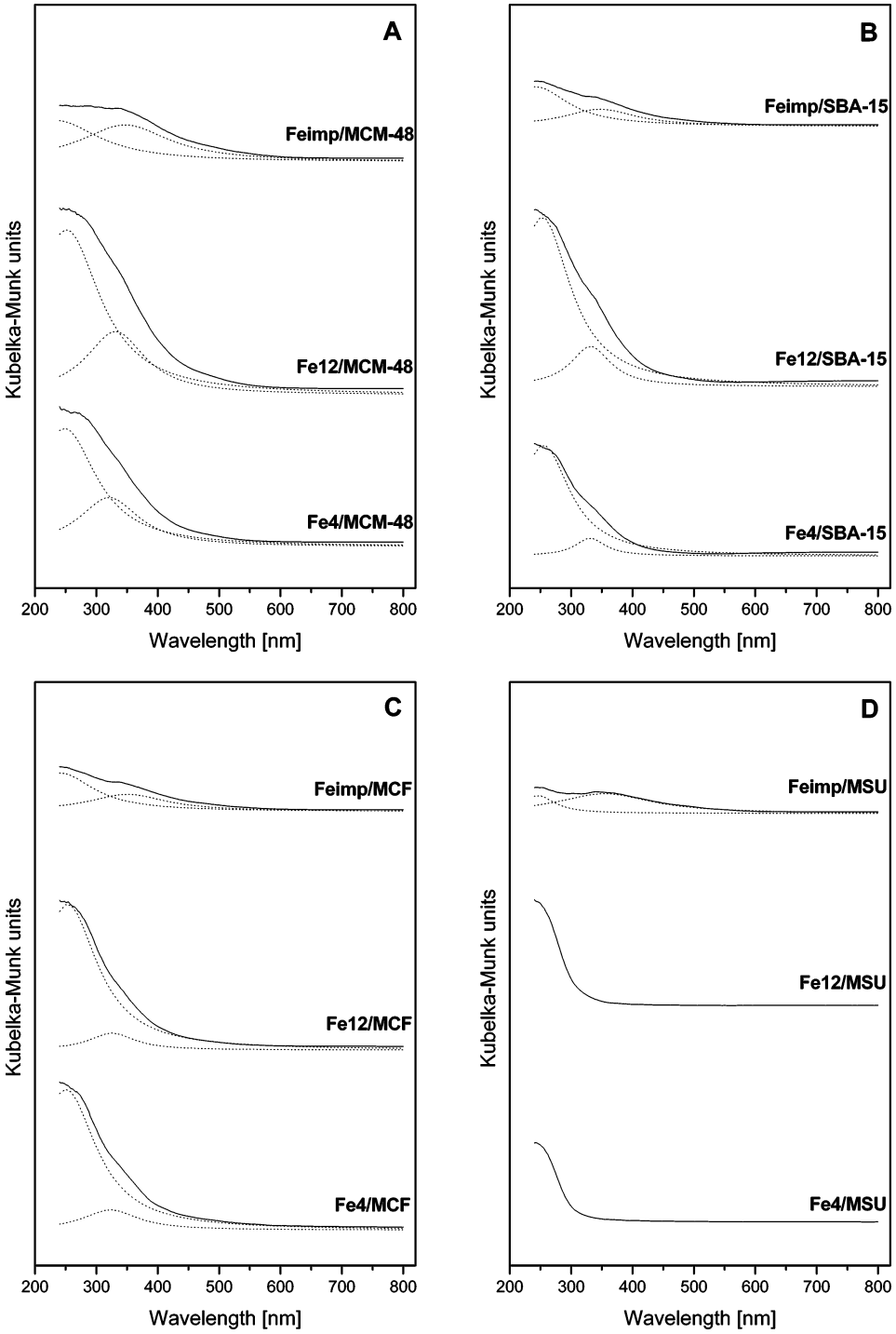

Figure 2. UV−vis diffuse reflectance spectra of mesoporous silicas MCM-48 (A), SBA-15 (B), MCF (C), and MSU (D) modified with iron oxide.

for 30 min in the flow of pure helium (grade 5). The TPR runs were carried out with the linear heating rate ($\beta = 10$ °C/min) in the flow of 2.0 vol % of H_2 in Ar (20 mL/min).

Catalytic Measurements. The synthesized catalysts were tested for the oxidative dehydrogenation of EB in the presence of nitrous oxide. The catalytic runs were performed in a plug flow microreactor (i.d., 6.0 mm and length, 240 mm). A total of 50 mg of the catalyst was loaded at the central position of the reactor onto a quartz wool plug. The flow of the gaseous reactants was controlled by mass flow controllers (Brooks 5850E). EB was fed into the system with a syringe pump (Cole-Parmer). The reaction products were monitored by a gas chromatograph (Varian CP-3800) equipped with three capillary columns: CP-8 (for separation of aromatic compounds), Poraplot Q (for CO_2, H_2O, and N_2O), Molsieve 5A (for N_2, O_2, and CO) and two detectors: TCD and mass spectrometer Saturn 2000 (Varian). A sample of reactants was always collected directly from the outlet of the reactor using a six-port valve (Valco).

Prior to the catalytic run, the sample was outgassed at 450 °C for 30 min in a flow of N_2O (0.4 mL/min) diluted with He (up to a total flow of 49.6 mL/min). Then, the dosing of EB (130 μL of liquid EB per hour) started. The first GC analysis was performed after 25 min. The temperature of the catalyst bed was increased from 450 to 550 °C in steps of 50 °C with three analyses of the obtained products (at 35 min intervals) at each step.

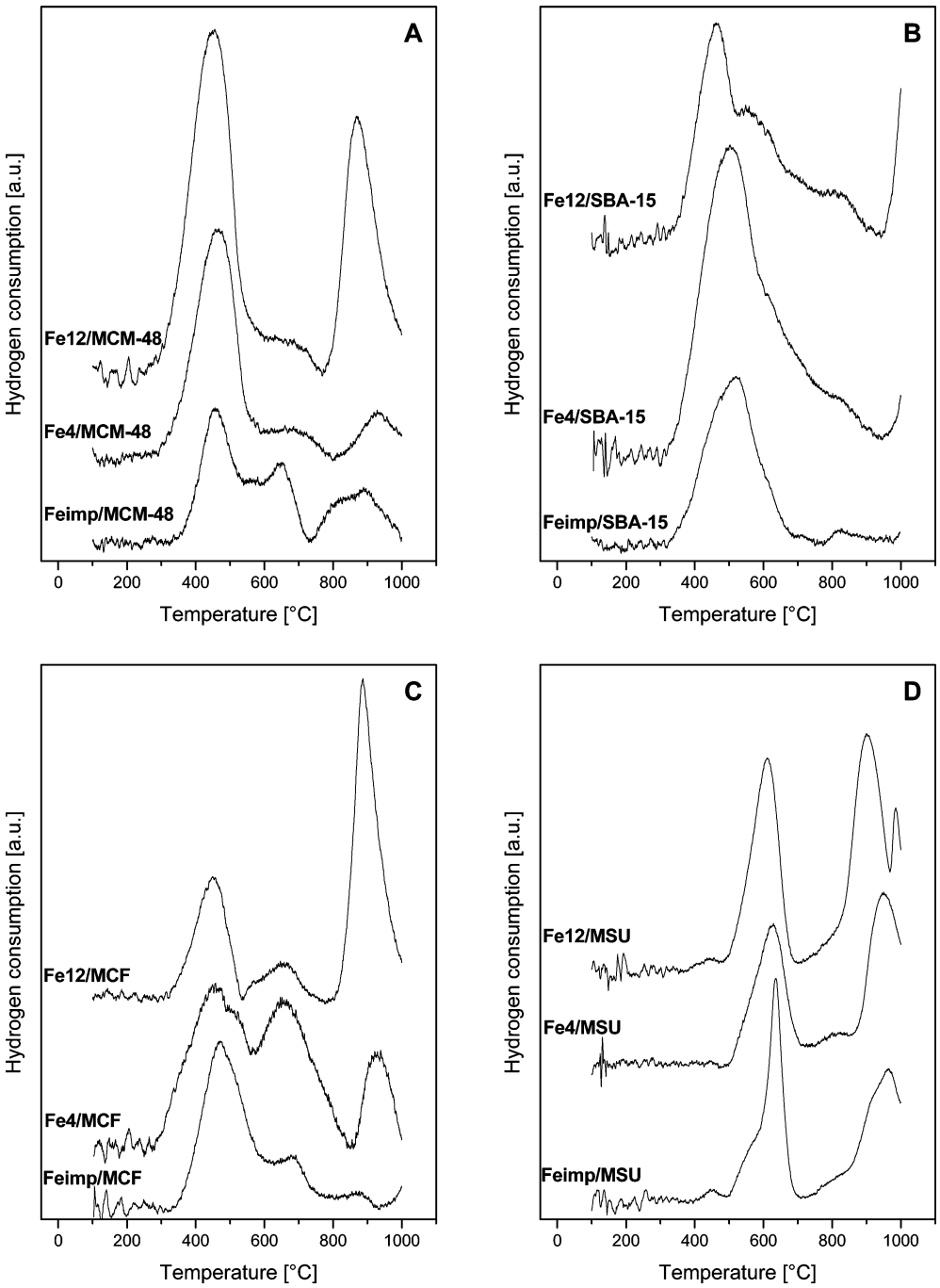

Figure 3. Temperature-programmed reduction (TPR) profiles of mesoporous silicas MCM-48 (A), SBA-15 (B), MCF (C), and MSU (D) modified with iron oxide.

Results and Discussion

In our recent work,[7] we have shown that the dispersion of iron on the mesoporous silica support is a crucial parameter influencing the catalytic performance of the Fe-containing catalysts in the oxidative dehydrogenation of EB with nitrous oxide. Isolated Fe^{3+} species appeared to be more effective in this process as compared to the oligomeric form of Fe. To obtain higher concentrations of isolated Fe^{3+} species on the mesoporous silicas, we decided to decrease an amount of Fe introduced by the impregnation technique from 3.0 to 1.0 wt. % or to use the MDD method for the Fe deposition. The mechanism of interaction of the $Fe(acac)_3$ complex with the mesoporous silica surface was discussed previously.[17] It was found that the low stability of iron acetylacetonate resulted in the ligand exchange between metal complex and silanol groups with the abstraction of one (for SBA-15, MCF, and MCM-48) or more (for MSU) molecules of Hacac.

The BET surface area (S_{BET}), total pore volume (V_{total}), and average pore diameter of the mesoporous samples before and after modification with iron are collected in Table 1. The presented data show the difference in the textural parameters of mesoporous silicas used as supports. For the nonmodified materials, the BET surface area sequence is MCM-48 > SBA-15 > MCF > MSU.

The MCM-48 silica with the highest surface area (909 m^2/g) is characterized by the presence of the smallest pores with a diameter of about 38 Å. The other mesoporous silicas possess significantly lower surface areas and wider pores. The pores consisting of a 3-D channel system in the MCF silica have diameters as high as 260 Å. It should, however, be kept in mind

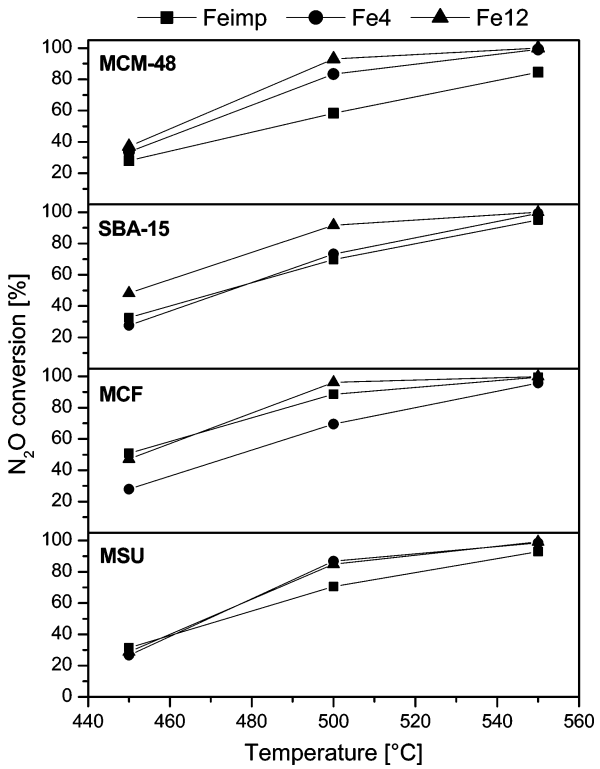

Figure 4. Conversion of N_2O vs the reaction temperature over different modified Fe-containing mesoporous catalysts.

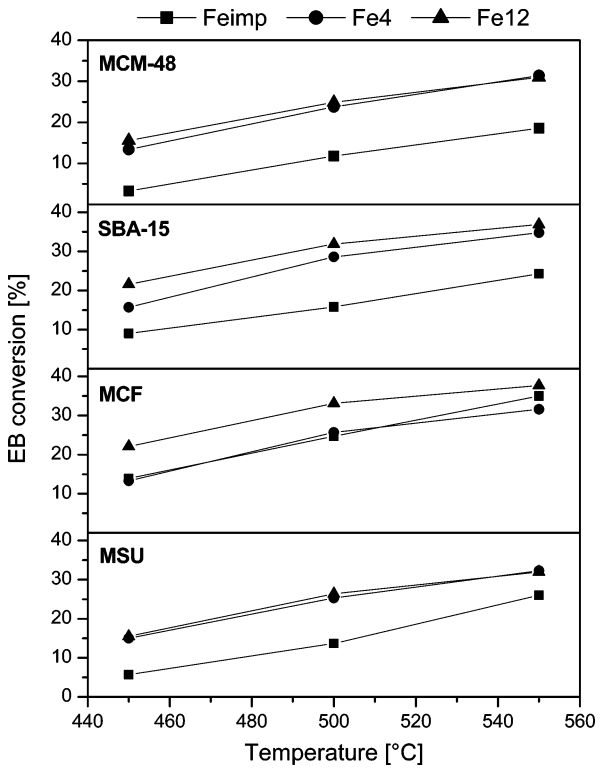

Figure 5. Conversion of ethylbenzene vs the reaction temperature over different modified Fe-containing mesoporous catalysts.

that such large spherical pores are interconnected by uniform windows with a considerably lower size.[15,18] The introduction of iron onto the mesoporous silica surface resulted in a decrease in both BET surface area and total pore volume. Moreover, the micropore volume of the SBA-15 support was reduced from 0.159 cm^3/g to 0.147 (Fe4/SBA-15), 0.140 (Fe12/SBA-15), and 0.135 cm^3/g (Feimp/SBA-15) after incorporation of iron species. No effect of a modification with Fe on the average pore diameter was observed. The most distinct changes in the textural parameters were found for the samples prepared by the impregnation technique. For the Feimp/MCM-48 catalyst, the surface area decreased by about 20% after the modification. It could be assumed that the observed changes are caused by a formation of Fe clusters partially blocking the pore system. However, the catalysts containing iron, obtained by the modification of mesoporous silicas, have still relatively high surface area and total pore volume.

In Table 1, the Fe loading was additionally presented. The samples modified by impregnation contain similar amounts of Fe (about 0.6−0.7 wt %), whereas the MDD method resulted in a higher Fe loading. The total Fe content depends strongly on the concentration of $Fe(acac)_3$ in toluene used for the deposition. An increase in the Fe acetylacetonate concentration resulted in a higher Fe content in the obtained catalysts.

The coordination environment of Fe in the calcined samples was studied by EPR spectroscopy. The recorded spectra for the Feimp/support and Fe12/support catalysts are shown in Figure 1. Generally, two signals, at $g = 2.0$ and 4.3, were detected. The EPR signal at $g = 2.0$ is usually attributed to Fe^{3+} ions in octahedral coordination forming iron oxide clusters;[19,20] however, isolated Fe^{3+} ions in positions of high symmetry contribute also to this line.[21,22] The line at $g = 4.3$ is typically assigned to tetrahedrally coordinated Fe^{3+} ions with strong rhombic distortion.[23,24]

UV−vis/DR spectroscopy was used to further investigate the nature of the Fe^{3+} species present in the mesoporous silica based catalysts. The spectra of the nonmodified supports showed only a very weak band centered at 250−270 nm attributed to structural Si in tetrahedral coordination.[7] The recorded spectra of the Fe-containing samples, as shown in Figure 2, were converted into Kubelka−Munk units and deconvoluted into Lorentzian subbands. Two bands, which can be assigned to the $d\pi-p\pi$ charge-transfer between iron and oxygen atoms, can be distinguished in the UV−vis/DR spectra of the Fe-modified catalysts. The band between 200 and 300 nm corresponds to isolated Fe^{3+} species, whereas the band in the range of 300−450 nm can be attributed to small oligonuclear $(FeO)_n$ species.[25−27] The performed deconvolution showed the contribution of both Fe forms. The highest relative content of isolated Fe^{3+} species was found for the samples modified by the MDD method (cf. Table 1). No significant difference in the contribution of isolated and cluster forms of Fe was observed for the catalysts obtained at various $Fe(acac)_3$ concentrations used for the deposition. It should be noticed, however, that the wider pore diameter favored the formation of the isolated form of Fe. The relatively high amounts of iron oxide clusters detected in the Fe4/MCM-48 and Fe12/MCM-48 catalysts give rise to a blocking of the pore system by an Fe deposition, which was concluded from the low-temperature N_2 adsorption measurements. On the other hand, a very high dispersion of Fe on the MSU support, obtained for the samples after grafting, could be attributed to the strong interaction between $Fe(acac)_3$ complex and surface silanols resulting in a loss of more than one acac ligand.[17]

The reducibility of the Fe-containing samples was studied by temperature-programmed reduction (TPR) with hydrogen. The collected TPR profiles are presented in Figure 3. The high dispersion of iron on the silica support causing that the reduction of Fe^{3+} ions begins at temperature as low as about 300 °C for the majority of catalysts based on the SBA-15, MCF, and MCM-48 materials. The Fe^{3+} species dispersed on the MSU support showed a higher stability in the reduction process and

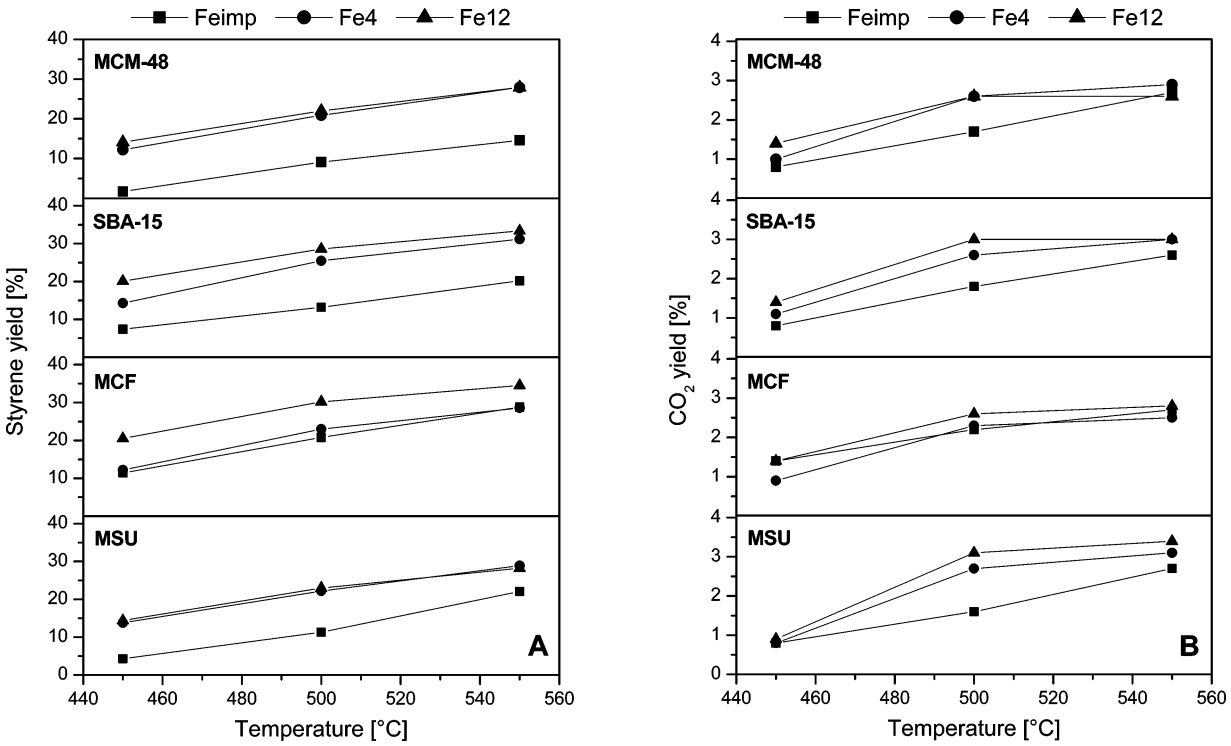

Figure 6. Yield of styrene (A) and CO_2 (B) vs the reaction temperature over different modified Fe-containing mesoporous catalysts.

were reduced starting from a temperature of 400−500 °C. Such strong stabilization of the Fe^{3+} oxidation state in this case should be explained by a nature of bonding of isolated Fe species to the MSU surface. As was discussed previously, Fe^{3+} ions deposited on the MSU material are mainly bounded by two covalent Fe−O−Si bonds. The TPR profiles recorded for the Fe-modified mesoporous silicas are very complex, which is obvious due to a different distribution of various forms of Fe^{3+} species inside the pores. Differences in the reduction mechanism of isolated and cluster Fe^{3+} species cannot be excluded. It should be noticed, however, that the samples modified by the grafting method exhibit the presence of hardly reducible Fe^{3+}, which begins to be reduced above 800 °C. The similar high-temperature effect of an iron reduction was observed for Fe^{3+} ions in the framework positions of zeolites.[25] Thus, it is most likely that grafting of Fe on the mesoporous silicas resulted in a partial incorporation of Fe into the SiO_2 matrix.

The MCM-48, SBA-15, MCF, and MSU mesoporous silicas modified with iron were tested as catalysts of the oxidative dehydrogenation of EB in the presence of N_2O. The conversion of N_2O and EB, used as reactants at the molar ratio of 1:1, is illustrated in Figures 4 and 5, respectively. It was observed that the Fe-containing catalysts were active even at temperature as low as 450 °C. The highest activity in the N_2O and EB conversion at 450 °C was found for the easiest reducible catalysts possessing relatively wide pores based on the SBA-15 and MCF materials. Furthermore, the obtained results that were found in the EB conversion showed that the catalytic activity is also influenced by Fe loading. A total of 48.3 and 47.2% of the N_2O conversion as well as 21.6 and 22.1% of the EB conversion was achieved at this temperature over the catalysts with the highest Fe content supported on SBA-15 (Fe12/SBA-15) and MCF (Fe12/MCF), respectively. An increase in the reaction temperature resulted in a gradual increase in the reactant conversion. At 550 °C, an almost total conversion of N_2O was observed over all the catalysts with the exception of the materials prepared by the impregnation method. Raising the reaction temperature to 550 °C enabled us to obtain also a high EB conversion, equal to 36.9 and 37.7%, for the most active Fe12/SBA-15 and Fe12/MCF catalysts. Furthermore, no significant decrease in the activity was observed during the catalytic runs. Therefore, it seems that coking, which was often the reason for a deactivation of the catalyst in the styrene production,[28] can be omitted when nitrous oxide was used as an oxidizing agent.

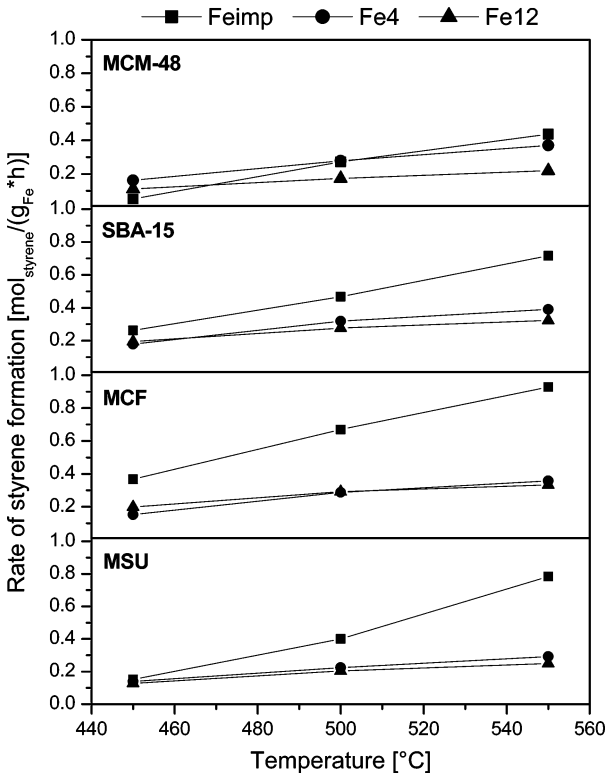

Figure 7. Rate of styrene formation related to the Fe content over various Fe-modified mesoporous silicas.

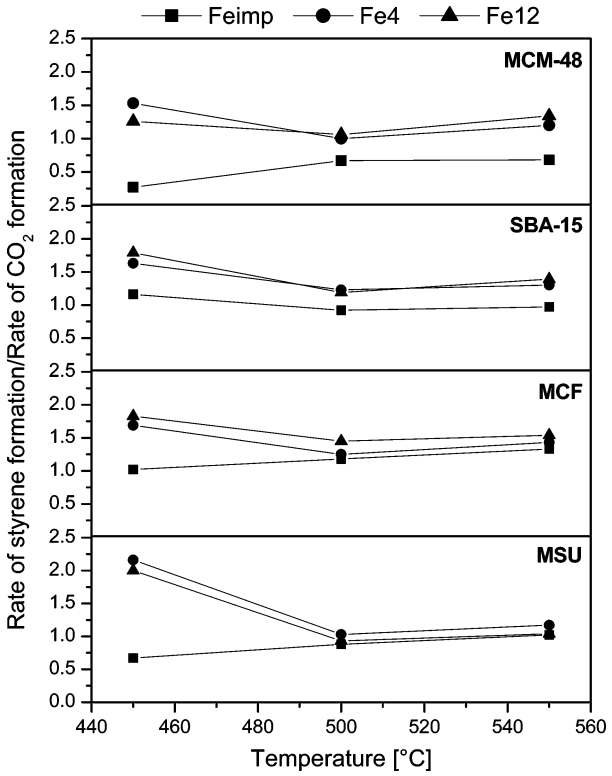

Figure 8. Ratio of styrene formation rate and CO_2 formation rate over various Fe-modified mesoporous silicas.

Styrene and CO_2 were the main carbon-containing products in the oxidative dehydrogenation of EB with N_2O. Only traces of CO and aromatic hydrocarbons (mainly benzene) were detected among the products. The yields of styrene and CO_2 in the function of the reaction temperature are presented in Figure 6 A,B, respectively. Similar to the EB conversion, an influence of the reducibility and Fe loading of catalysts on the main product yields was found. Taking into account the difference in the Fe content, the effectiveness of the catalysts can be determined when the catalytic performance is expressed in the terms of the rate of product formation ($mol_{product}\ h^{-1}$) related to the Fe content (g_{Fe}). The calculated styrene formation rate for the oxidative dehydrogenation of EB in the presence of nitrous oxide over the Fe-modified mesoporous silicas is shown in Figure 7, whereas the comparison of the rates of styrene and CO_2 formation is presented in Figure 8. The samples modified by the MDD method showed very similar activities in the dehydrogenation of EB to styrene. However, a considerable difference in the styrene rate formation was found for the catalysts obtained by the impregnation and grafting methods. Fe supported on mesoporous silicas by the impregnation technique appeared to be significantly more effective in the styrene production. On the other hand, these catalysts were also active in the total oxidation of aromatics. The comparison of selectivity toward styrene and CO_2 (cf. Figure 8) reveals that the Feimp/support samples are more selective for the total oxidation to CO_2 than for the EB dehydrogenation. Such catalytic behavior should be assigned to the dominate form in which Fe is present on the catalyst surface. It could be concluded that the isolated Fe^{3+} species are less active in the oxidation of ethylbenzene and more selective in the dehydrogenation of EB to styrene as compared to the cluster-type iron oxide. It is most likely that the process proceeds according to the Mars−van Krevellen mechanism. In the first step, EB is partially oxidized to styrene by lattice oxygen

$$EB + FeO_x \rightarrow \text{styrene} + FeO_{x-1} + H_2O$$

In the subsequent step, the reduced Fe surface species is reoxidized by N_2O

$$FeO_{x-1} + N_2O \rightarrow FeO_x + N_2.$$

The presence of an easily reducible oxide system is therefore one of the important factors influencing the catalytic activity in the studied process. However, the Fe^{3+} oxide species presenting suitable redox properties should be rather highly dispersed on the support surface than agglomerated in the cluster-type arrangement. In the case of the presence of Fe oxide clusters, the excess of lattice oxygen originating from N_2O decomposition is so high that it can easily oxidize EB to CO_2.

Conclusion

The impregnation and molecular designed dispersion are methods useful for introduction of iron onto the mesoporous silica supports. However, the choice of deposition technique and type of mesoporous silica plays a role in the dispersion of Fe^{3+} species onto the support surface. Obtaining high Fe dispersion demands wide pore mesoporous silica as a raw material and grafting for the deposition of iron. The UV−vis/DRS measurements showed that the highest amount of isolated Fe^{3+} species was obtained for the SBA-15, MCF, and MSU samples modified by the MDD method. On the other hand, a part of Fe^{3+} ions grafted on the silica surface is strongly stabilized in their oxidation state and can only be reduced by hydrogen at a temperature exceeding 800 °C.

The Fe-containing mesoporous silicas were found to be active catalysts for the oxidative dehydrogenation of EB to styrene in the presence of nitrous oxide. It was observed that the easily reducible samples showed the highest catalytic performance in this process. However, the reaction selectivity depended strongly on the chemical environment of Fe. Isolated Fe^{3+} species appeared to be more selective in the styrene formation, whereas iron oxide clusters showed a higher selectivity in the total oxidation of aromatic hydrocarbons. It could be concluded that the process proceeds according to the Mars−van Krevellen mechanism and that lattice oxygen plays a role as a real oxidizing agent.

Acknowledgment. The authors thank the Ministry of Flanders and the Polish Ministry of Scientific Research and Information Technology for financial support in the frame of a bilateral Flemish−Polish project for 2004−2005.

Supporting Information Available: Figures showing nitrogen adsorption−desorption isotherms and pore size distributions. This material is available free of charge via the Internet at http://pubs.acs.org.

References and Notes

(1) Lee, E. H. *Catal. Rev.* **1973**, *8*, 285.
(2) Cavani, F.; Trifirò, F. *Appl. Catal. A* **1995**, *133*, 219.
(3) Emig, G.; Hofmann, H. *J. Catal.* **1983**, *84*, 15.
(4) Vrieland, G. E.; Menon, P. G. *Appl. Catal.* **1991**, *77*, 1.
(5) Lisovskii, A. E.; Aharoni, C. *Catal. Rev.—Sci. Eng.* **1994**, *36*, 25.
(6) Kuśtrowski, P.; Zbroja, M.; Dziembaj, R.; Papp, H. *Catal. Lett.* **2002**, *80*, 1.
(7) Kuśtrowski, P.; Chmielarz, L.; Dziembaj, R.; Cool, P.; Vansant, E. F. *J. Phys. Chem. A* **2005**, *109*, 330.
(8) Kenvin, J. C.; White, M. G.; Mitchell, M. B. *Langmuir* **1991**, *7*, 1198.
(9) Van Der Voort, P.; Possemiers, K.; Vansant, E. F. *J. Chem. Soc., Faraday Trans.* **1996**, *92*, 843.

(10) Van Der Voort, P.; Babitch, I. B.; Grobet, P. J.; Verberckmoes, A. A.; Vansant, E. F. *J. Chem. Soc., Faraday Trans.* **1996**, *92*, 3635.
(11) Van Der Voort, P.; Baltes, M.; Vansant, E. F.; White, M. G. *Interface Sci.* **1997**, *5*, 209.
(12) Baltes, M.; Collart, O.; Van Der Voort, P.; Vansant, E. F. *Langmuir* **1999**, *15*, 5841.
(13) Collart, O.; Van Der Voort, P.; Vansant, E. F.; Desplantier, D.; Galarneau, A.; Di Renzo, F.; Fajula, F. *J. Phys. Chem. B* **2001**, *105*, 12771.
(14) Van Bavel, E.; Cool, P.; Aerts, K.; Vansant, E. F. *J. Phys. Chem. B* **2004**, *108*, 5263.
(15) Schmidt-Winkel, P.; Lukens, W. W.; Zhao, D.; Yang, P.; Chmelka, B. F.; Stucky, G. D. *J. Am. Chem. Soc.* **1999**, *121*, 254.
(16) Kim, S. S.; Karkamkar, A.; Pinnavaia, T. J.; Kruk, M.; Jaroniec, M. *J. Phys. Chem. B* **2001**, *105*, 7663.
(17) Kuśtrowski, P.; Chmielarz, L.; Dziembaj, R.; Cool, P.; Vansant, E. F. *J. Phys. Chem. B* **2005**, *109*, 11552.
(18) Lettow, J. S.; Han, Y. J.; Schmidt-Winkel, P.; Yang, P.; Zhao, D.; Stucky, G. D.; Ying, J. Y. *Langmuir* **2000**, *16*, 8291.
(19) Derouane, E. G.; Mestsdagh, M.; Vielvoye, L. *J. Catal.* **1974**, *33*, 169.
(20) Savidha, R.; Pandurangan, A. *Appl. Catal. A* **2004**, *276*, 39.
(21) Brückner, A.; Lohse, U.; Mehner, H. *Microporous Mesoporous Mater.* **1998**, *20*, 207.
(22) Pérez-Ramírez, J.; Kumar, M. S.; Brückner, A. *J. Catal.* **2004**, *223*, 13.
(23) Aasa, R. *J. Chem. Phys.* **1983**, *52*, 3919.
(24) Wang, Y.; Zhang, Q.; Shishido, T.; Takehira, K. *J. Catal.* **2002**, *209*, 186.
(25) Bordiga, S.; Buzzoni, R.; Geobaldo, F.; Lamberti, C.; Giamello, E.; Zecchina, A.; Leofanti, G.; Petrini, G.; Tozzolo, G.; Vlaic, G. *J. Catal.* **1996**, *158*, 486.
(26) Pérez-Ramírez, J.; Kapteijn, F.; Brückner, A. *J. Catal.* **2003**, *218*, 234.
(27) Yu, Y.; Xiong, G.; Li, C.; Xiao, F. S. *J. Catal.* **2000**, *194*, 487.
(28) Dziembaj, R.; Kuśtrowski, P.; Badstube, T.; Papp, H. *Top. Catal.* **2000**, *11/12*, 317.